An automatic pipeline for the design of irreversible derivatives identifies a potent SARS-CoV-2 M^{pro} inhibitor.

Daniel Zaidman[1,*], Paul Gehrtz[1,*], Mihajlo Filep[1], Daren Fearon[2], Jaime Prilusky[3], Shirly Duberstein[4], Galit Cohen[4], David Owen[2,5], Efrat Resnick[1], Claire Strain-Damerell[2,5], Petra Lukacik[2,5], Covid-Moonshot Consortium, Haim Barr[4], Martin A. Walsh[2,5], Frank von Delft[2,5,6,7], Nir London[1,#]

[1] Dept. of Organic Chemistry, Weizmann Institute of Science, 7610001, Rehovot, Israel

[2] Diamond Light Source Ltd., Harwell Science and Innovation Campus, Didcot OX11 0QX, U.K.

[3] Life Sciences Core Facilities, Weizmann Institute of Science, 7610001, Rehovot, Israel

[4] Wohl Institute for Drug Discovery of the Nancy and Stephen Grand Israel National Center for Personalized Medicine, The Weizmann Institute of Science, Rehovot, 7610001, Israel

[5] Research Complex at Harwell, Harwell Science and Innovation Campus, Didcot OX11 0FA, U.K.

[6] Structural Genomics Consortium, University of Oxford, Old Road Campus, Roosevelt Drive, Headington, OX3 7DQ, UK

[7] Department of Biochemistry, University of Johannesburg, Auckland Park 2006, South Africa

[*] Equal contribution

[#] Corresponding author: nir.london@weizmann.ac.il

27   **Abstract**

28   Designing covalent inhibitors is a task of increasing importance in drug discovery. Efficiently
29   designing irreversible inhibitors, though, remains challenging. Here, we present *covalentizer*, a
30   computational pipeline for creating irreversible inhibitors based on complex structures of targets
31   with known reversible binders. For each ligand, we create a custom-made focused library of
32   covalent analogs. We use covalent docking, to dock these tailored covalent libraries and to find
33   those that can bind covalently to a nearby cysteine while keeping some of the main interactions of
34   the original molecule. We found ~11,000 cysteines in close proximity to a ligand across 8,386
35   protein-ligand complexes in the PDB. Of these, the protocol identified 1,553 structures with
36   covalent predictions. In prospective evaluation against a panel of kinases, five out of nine predicted
37   covalent inhibitors showed IC_{50} between 155 nM - 4.2 μM. Application of the protocol to an
38   existing SARS-CoV-1 M^{pro} reversible inhibitor led to a new acrylamide inhibitor series with low
39   micromolar IC_{50} against SARS-CoV-2 M^{pro}. The docking prediction was validated by 11 co-crystal
40   structures. This is a promising lead series for COVID-19 antivirals. Together these examples hint
41   at the vast number of covalent inhibitors accessible through our protocol.

42

Introduction

Covalent irreversible inhibitors have become increasingly popular over the last decade as chemical probes and drugs. Most often these inhibitors target a cysteine residue to form the covalent bond. Several rationally-designed irreversible inhibitors targeting cysteines were approved by the FDA in recent years, with notable examples such as Ibrutinib[1], Afatinib[2] and Osimertinib[3]. Irreversible binding offers a variety of advantages, including prolonged residence time[4] and an ability to compete with high-affinity natural substrates[5–7]. Another important advantage of covalent inhibitors is their improved selectivity when targeting non-conserved cysteine residues[8,9]. Moreover, covalent binding can enable targeting of especially challenging targets such as the G12C oncogenic K-Ras mutation[10–12].

Historically, most covalent inhibitors were designed by the addition of an electrophile to an already known reversible inhibitor that suitably binds next to a cysteine residue[13–18]. More recently, covalent inhibitors are also being discovered by empirical screening of covalent fragment libraries[19–25] and by covalent virtual screening[10,26–32]. While covalent fragment and virtual screening can potentially discover new scaffolds, the binding affinity of primary hits may be relatively low, and often require laborious medicinal chemistry to reach suitable potency.

Covalent derivatization of an already known reversible binder, can endow the compound with added benefits of irreversible binding such as time dependent inhibition, longer duration of action, improved selectivity towards proteins that contain the target cysteine compared to homologs without a cysteine at that position, and possibly improved potency. Still, this approach is far from trivial. Three crucial questions have to be answered: 1. Which electrophilic moiety to use? 2. What is the optimal vector on the scaffold to attach through? 3. What linker, if any, would optimize the placement of the electrophile with respect to the binding mode of the scaffold and the position of the target cysteine residue? There are numerous possible answers for these questions. Furthermore, the "*covalentized*" (derivative containing the electrophile) version of the reversible inhibitor should be synthetically accessible. Therefore, tools that would enable to address this design problem algorithmically, would significantly simplify covalent inhibitor design and has the potential to discover many potent covalent binders for a large variety of targets.

Computational approaches to address this challenge are scarce. DUckCov[29] a covalent virtual screening method, begins with non-covalent docking of a library of covalent compounds, while using pharmacophoric constraints for hydrogen bonds, as well as for the covalent warhead. This is followed by covalent docking of the ligands with the strongest non-covalent affinities. CovaDOTS[33] uses a set of synthetic schemes and available building blocks, to create covalent analogs of existing non-covalent ligands, but was only assessed retrospectively. Cov_FB3D[34] constructs *de novo* covalent ligands and was retrospectively assessed on recapitulation on known covalent inhibitors.

Here we present a computational pipeline to identify potential existing reversible binders for *covalentization* (creation of a covalent analog). Given a complex structure or model of a ligand in the vicinity of a cysteine residue, we elaborate the ligand or its substructures with various

83   electrophiles. This *ad hoc* library of covalent analogs is covalently docked to the target protein and
84   the original (non-covalent) structure is used as a filter to identify high-confidence covalent
85   candidates. We applied this protocol - *covalentizer* - to the entire PDB to identify thousands of
86   potential candidates amenable for irreversible inhibition, and made both the protocol and the
87   database of pre-computed candidates publicly available to the community
88   (https://covalentizer.weizmann.ac.il). We have prospectively synthesized and tested several
89   predictions of various covalent kinase inhibitors proposed by the protocol and succeeded in five
90   out of nine designs with IC_{50}'s of 155 nM - 4.2 μM.

91   In early February 2020, the COVID-19 pandemic started to spread globally[35,36]. We turned
92   to the pre-compiled database of *covalentizer* results, to look for possible candidate inhibitors for
93   SARS-CoV-2 proteins. The search found a reversible small molecule inhibitor designed against
94   the main protease of the SARS-CoV-1 virus (PDB: 3V3M[37]), which has 96% sequence identity to
95   the main protease of SARS-CoV-2, with a promising covalent prediction. We synthesized the
96   prediction and validated irreversible binding to the SARS-CoV-2 main protease (M^{pro}). We further
97   optimised the non-covalent affinity of the compound, resulting in improved analogs. Co-crystal
98   structures confirmed the computational model. This example highlights the strength of our method
99   - the design was already available, and enabled very rapid development. The database suggests
100   that hundreds more such examples await testing.

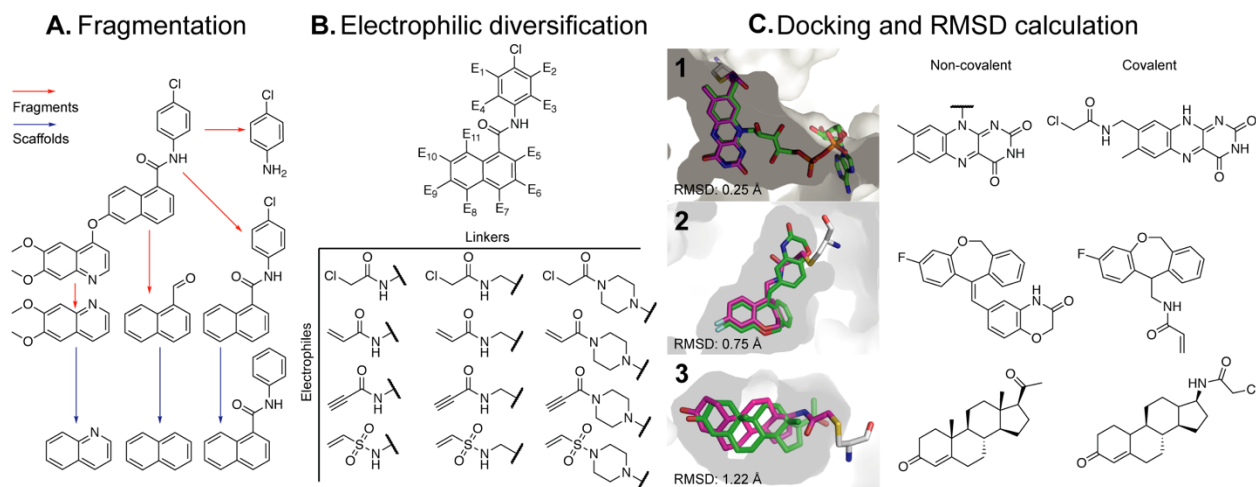101

102   **Results**

103

104   *The covalentizer pipeline*

105

106   For a given complex structure with a reversible ligand in the vicinity of a target cysteine
107   residue, the pipeline (Fig. 1) comprises four consecutive steps: fragmentation, electrophile
108   diversification, covalent docking and RMSD filtering.

109

110
111   **Figure 1. An overview of the *covalentizer* computational protocol.**
112   The protocol comprises four consecutive steps. **A.** Fragmentation: the molecule is broken and divided into fragments
113   (red arrows) using synthetically accessible bonds[38]. Murcko scaffolds[39] of the fragments (blue arrows) are also added
114   to the list of fragments. **B.** Electrophilic diversification: for each substructure, a library of potential electrophilic
115   analogs is generated, a few hundred compounds in size. We used four kinds of nitrogen-based electrophiles ranging
116   in reactivity: vinyl sulfones, chloroacetamides, acrylamides and propynamides. We also considered various linkers
117   between the fragment and the electrophile. **C.** Docking: The target structure is then docked against its appropriate
118   analog library using all available cysteine rotamers. Finally, RMSD calculation: For each docked compound, an
119   RMSD is calculated between the MCS (maximal common substructure) of the reversible compound and the new
120   covalent analog. We show examples of predictions with increasing RMSDs, for binders of 1. Nitrate reductase from
121   Ulva prolifera (PDB: 5YLY) 2. Human mineralocorticoid receptor (PDB: 5HCV) and 3. Human progesterone receptor
122   (PDB: 1A28).

123

124   A. Fragmentation: In this step, the ligand is broken-down and divided into two parts via
125   synthetically accessible bonds[38]. Doing this recursively, results in a list of substructures (Fig. 1A).
126   For each substructure, we augment the list with its corresponding Murcko scaffold[39] (the naked
127   ring system, without any decoration) to allow more exit vectors from which the electrophile can
128   be added next. The motivation for this fragmentation step is three-fold. First, as mentioned,
129   fragmenting the molecule exposes new vectors on which to install the electrophile (see Fig. 1C
130   example 2). Second, the additional constraint of forming the covalent bond might cause a slight
131   shift to the molecule's binding mode from the original crystal structure. Such a shift may propagate
132   and cause a steric clash between the protein and a ligand moiety distal to the electrophile. Since
133   adding the covalent bond is expected to increase the overall potency, we 'sacrifice' parts of the

134   molecule to enable the addition of an electrophile. The final ranking of candidate covalent analogs
135   relies on covalent docking which is sensitive to sub-Å shifts. Hence, occasionally, a truncated
136   version of the ligand will dock well, while the full ligand will not. Thus, including the sub-
137   structures and their scaffolds maximizes the number of candidates. Since covalent docking
138   accuracy was shown to deteriorate with ligand size and number of rotatable bonds[26], we filter the
139   final list of substructures, to those with 8-25 heavy atoms and up to five rotatable bonds.

140

141   B. Electrophile diversification: For each substructure or scaffold, we generate a library of potential
142   electrophilic analogs, typically resulting in a few hundred analogs (Fig. 1B). We consider four
143   kinds of electrophiles ranging in reactivity: vinyl sulfonamides, chloroacetamides, acrylamides
144   and propynamides, that can all be installed in one step onto a free amine. We add these
145   electrophiles to the substructures using simple connection rules which, however, do not guarantee
146   synthetic accessibility (see methods section for more details). We also consider various linkers
147   between the fragment and the electrophile. In our application below, we considered either a
148   methylene linker or various di-amine linkers (Supp. Fig. 1).

149

150   C. Covalent docking: The structure of the complex is prepared for docking, using all available
151   cysteine rotamers. We use DOCKovalent[26] to dock the electrophile library we described above
152   against the protein (after removing the crystallographic ligand).

153

154   D. RMSD filtering: Compounds that are able to form a covalent bond with the target cysteine while
155   still maintaining the same binding mode of the original reversible ligand are likely candidates for
156   covalent analogs. To assess this, we evaluate the RMSD (root mean square deviation) between
157   each docking prediction and the crystallographic ligand. Due to the fact that RMSD is calculated
158   between two sets of matching atoms, and the reversible ligand is different from the irreversible
159   one, it was calculated based on the maximal common substructure (MCS) between the two
160   molecules. Figure 1C exemplifies predictions with varying RMSDs. For a PDB wide application
161   of the pipeline, we focused on covalent analogs with a docking position of < 1.5 Å RMSD from
162   the crystallographic ligand.

163

164   *Covalent kinase inhibitors benchmark*

165

166   To benchmark the pipeline, we wanted to test whether it is able to find known covalent inhibitors,
167   given only their reversible part as input. To achieve this, we used the kinase subset of a recently
168   published covalent docking benchmark[30]. This set included 35 kinase covalent inhibitor complex
169   structures with either acrylamides, chloroacetamides or vinyl sulfonamides (after excluding seven
170   inhibitors with uncommon electrophiles). To form the input for *covalentizer*, we removed the
171   electrophiles while leaving only a free amine. For substituted acrylamides we removed β-
172   substitutions as well.

173   Out of the 35 structures, the pipeline identified the crystallographic covalent inhibitor in
174   14 (40%) of the cases, with a threshold of 1.5 Å MCS-RMSD (Fig. 2; Supp. Table 1).
175
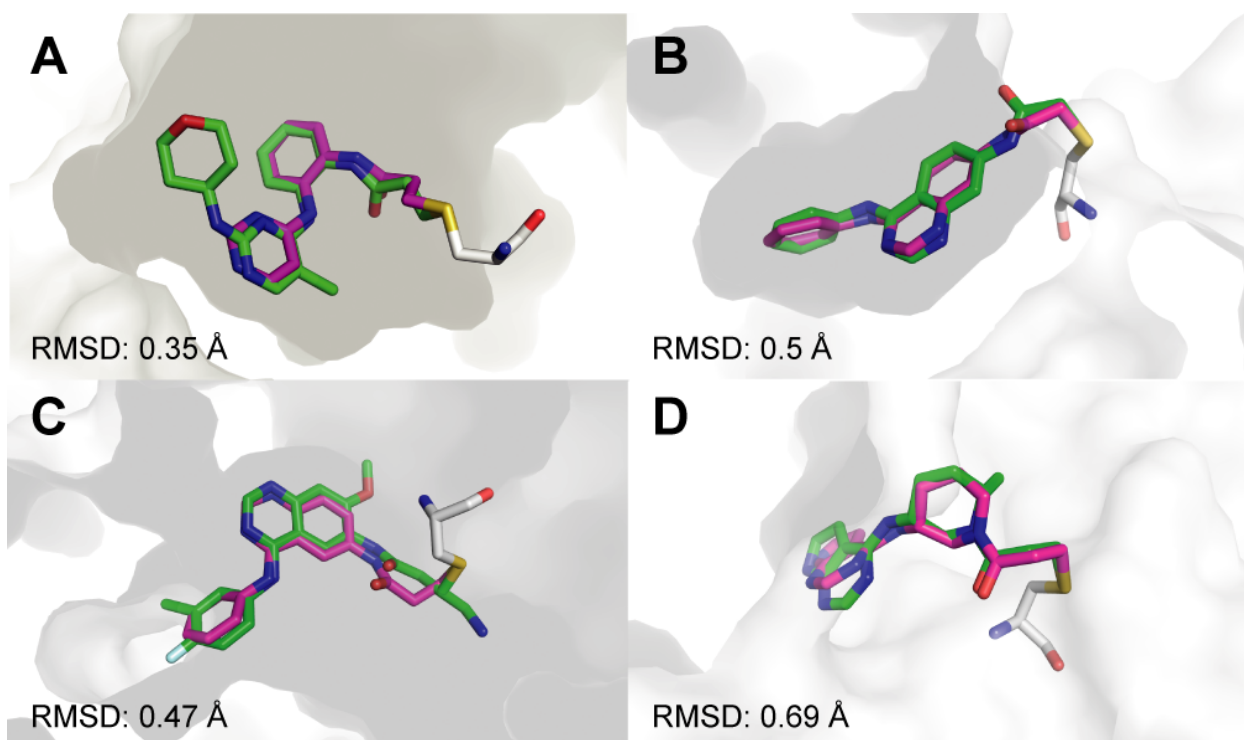
176
177   **Figure 2. *Covalentizer* successfully recapitulates known covalent kinase inhibitors.**
178   Examples of covalent kinase inhibitors (green) for which *covalentizer* was able to find a substructure match (magenta)
179   under the 1.5 Å threshold. **A.** ERK2, PDB: 4ZZO. **B.** EphB3, PDB: 5L6P. **C.** EGFR (T790M), PDB: 4I24. **D.** JAK3,
180   PDB: 5TOZ. The electrophiles span acrylamides (A,D), a substituted acrylamide (C) and chloroacetamide (B).
181

182   *Covalentizing the PDB*

183

184   Encouraged by the results in recapitulating known covalent kinase inhibitors we aimed to
185   apply our protocol to the entire PDB. We started from the set of all the protein-small molecule X-
186   ray structures (< 3.0 Å resolution) that contained a small molecule with a molecular weight greater
187   than 300 Da, and no DNA/RNA chains. As of the date of the search (July 4th, 2019) this resulted
188   in 44,990 structures. We filtered these to structures in which a ligand has one of its atoms within
189   6 Å of the sulphur atom of a free cysteine residue. Disulfides or covalently modified cysteines
190   were excluded. After applying this filter, we ended up with 8,386 such structures, and ~11,000
191   cysteines.

192   These structures, which constitute the target space for our protocol, contain significant
193   redundancy. Clustering them with a threshold of 90% sequence identity, results in 2,227
194   representatives. 38% of the structures are of human proteins and the rest span many other
195   organisms including rodents, bacteria and yeast. They also span seven different enzyme classes,
196   with the most prevalent being transferases (41.4%). 928 structures (11.1% of the entire dataset)

197 are kinases. These ~8,400 proteins contain 3,673 different ligands, each binding next to a cysteine.
198 The ligand that is most abundant in this database is Flavin-Adenine Dinucleotide occurring in 504
199 structures, whereas 3,058 ligands (83% of the compounds) occur only in a single structure. The
200 most common ligands were nucleotide or nucleotide-like molecules.

201 After running the aforementioned algorithm against the ~8,400 structures that passed our
202 filtering (Fig 3A), 1,553 structures produced at least one candidate below the 1.5 Å RMSD cutoff.
203 These structures represent roughly 380 proteins (representative set at 95% sequence identity).
204 1,051 structures are of human proteins, 338 are structures of kinases. 80 of the structures had
205 produced a covalent analog prediction that was docked < 0.5 Å from the original ligand,
206 representing very high-confidence candidates (Fig. 3B). The distribution of selected electrophiles
207 is almost uniform (Fig. 3C). All of the predictions are made available through a public website
208 (https://covalentizer.weizmann.ac.il) which is automatically updated weekly with new PDB
209 entries.
210
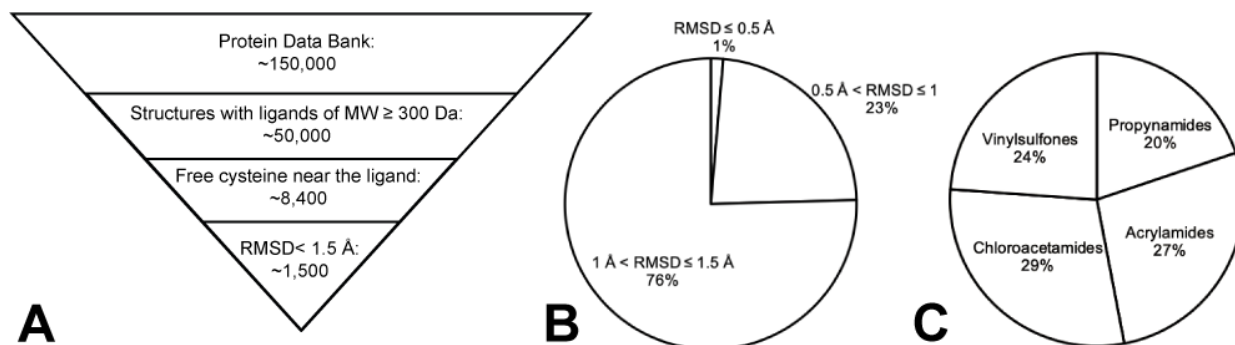
211
212 **Figure 3. PDB wide application of *covalentizer* identifies candidate irreversible inhibitors for more than 1,500**
213 **structures. A.** We filtered the protein data bank (PDB) for structures that had only protein chains (no DNA/RNA),
214 and contained a small molecule of at least 300 Da. This threshold was set to ensure some minimal initial fit/binding
215 affinity to the target, as well as to filter out non-ligand small molecules like crystallization reagents. We used a pymol
216 based script to filter only the structures in which at least one ligand atom is < 6 Å away from the sulfur atom of a
217 cysteine residue. This cysteine also has to be free (no disulfide or other covalent modifications). After running the
218 *covalentizer* protocol and filtering only for results with < 1.5 Å RMSD of the maximal common substructure (MCS)
219 between the reversible ligand and the covalent analog generated by *covalentizer*, there were 1,553 structures for which
220 at least one such prediction was obtained. **B.** The top 1% of results have an RMSD under 0.5 Å. 23% are between 0.5
221 Å and 1 Å, and 76% are between 1 Å and 1.5 Å. **C.** The distribution of the four electrophiles used is balanced, with
222 29% chloroacetamides, 27% acrylamides, 24% vinylsulfones, and 20% propynamides.
223

224 *Exploring additional linkers*
225

226 As mentioned above, the entire database was processed using direct attachments of the
227 electrophiles to atoms of the sub-structures, as well as with a methylene linker. The use of longer
228 and more diverse linkers for the addition of an electrophile would allow the targeting of cysteines
229 further from the ligand thus increasing the available target space, as well as diversifying the
230 introduced chemistry. To investigate this further, we searched the covalent inhibitor discovery
231 literature[40–43] for the most common di-amine linkers used in the last decade which led to the

232   selection of 7 aromatic linkers and 17 aliphatic linkers (Supp. Fig. 1). Since including all of these
233   linkers increases the computational demands of the pipeline, we restricted its application to the
234   subset of liganded kinase structures in the PDB. Since these linkers can enable ligands to reach
235   further cysteines at extended distances, the search criteria was extended to a distance of up to 10
236   Å from the ligand (instead of 6 Å, previously).
237   The final subset includes 1,880 PDB structures that contain a Cys residue of up to 10 Å
238   away from one of 1,398 various ligands. The size of the custom-made libraries of electrophilic
239   analogs for a particular reversible ligand, containing these linkers, now extends to a few thousand
240   compounds. Overall, we generated *in silico* over 3 million electrophilic compounds with di-amine
241   linkers for the kinase subset. The results show candidates of < 1.5 Å MCS-RMSD between the
242   original reversible ligand and the electrophilic candidate for 411 protein structures. 186 of these
243   structures (45%) were not found in the previous run, showing the potential of using these more
244   sophisticated linkers to reach farther cysteines and to *covalentize* more ligands.
245
246   *Novel covalent inhibitors for various kinases*
247
248   Kinase inhibitors comprise 22% of the *covalentizer* results. We selected a subset of these
249   for prospective validation. We chose the candidates based on three features: 1. Low RMSD relative
250   to the parent reversible ligand. 2. The addition of the electrophile is not predicted to interfere with
251   the kinase hinge binding region. 3. Ease of synthesis. This required manual inspection of pre-
252   selected low RMSD results. Overall, we made and tested nine compounds (Fig. 4) targeting five
253   different kinases. In some cases, addition of the electrophile required removal of large parts of the
254   parent reversible ligand (Supp. Fig. 2). The compounds were each tested in a kinase activity assay
255   against the target kinase in the structure from which the *covalentizer* result was derived. The assay
256   was performed at ATP concentration equal to the K_m of the kinase in question, with a 2 h pre-
257   incubation of the inhibitor at 25 °C.
258
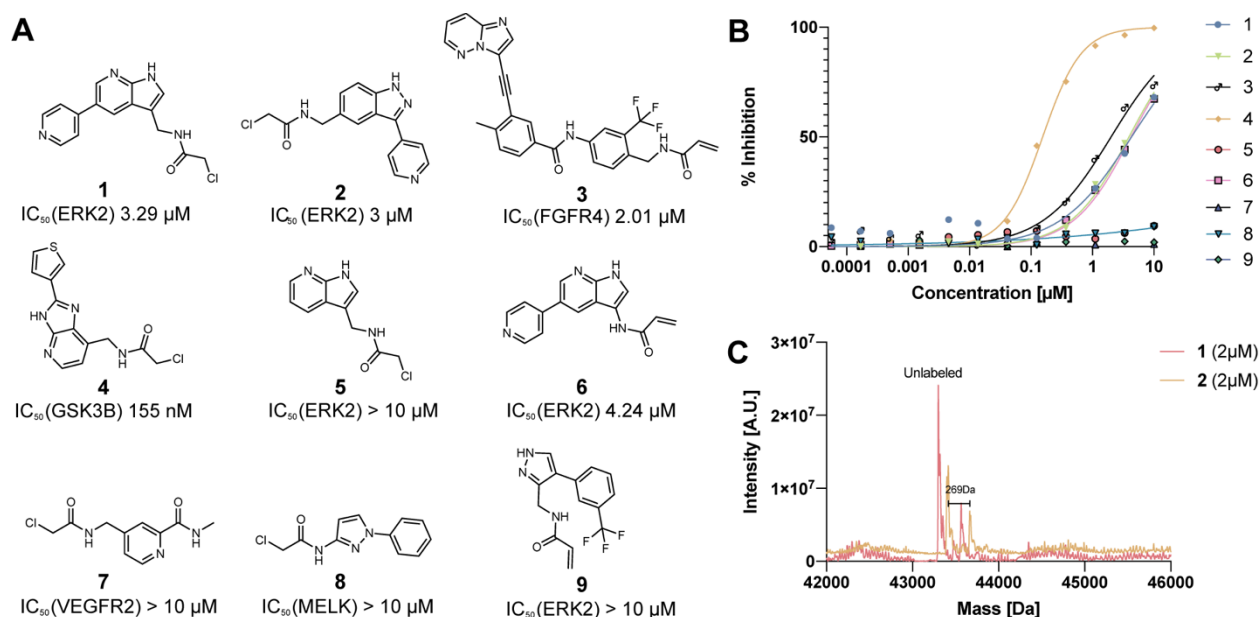
Figure 4. Prospective prediction identifies novel irreversible kinase inhibitors. A. Chemical structures and in vitro kinase activity assay $IC_{50}s$ for nine prospective *covalentizer* predictions. See Supp. Fig. 2 for the parent compounds, pose predictions and RMSD values. **B.** Dose response curves for each of the nine compounds (see additional repetitions for **1** and **2** in Supp. Fig. 3). Each compound was tested against its corresponding target kinase. **C.** Deconvoluted mass spectra obtained by intact protein LC/MS of recombinant ERK2 (2 µM) incubated with equimolar **1** or **2** for 1 h at room temperature, identifies significant irreversible binding by both compounds.

Four of the nine compounds did not show inhibition under the assay conditions (IC_{50} > 10 µM). Three compounds targeting ERK2 showed IC_{50} values of 3 - 4.24 µM. For two of these inhibitors, **1** and **2**, we assessed irreversible binding to ERK2 by intact protein mass spectrometry (2 µM ERK2, 2 µM compound, 1 h incubation at 25 °C). The expected protein-compound adducts were detected (25% and 33% labeling respectively; peak-to-peak Δm 265-270 Da for both compounds; Fig. 4B) with no additional adducts derived from multiple reactions, highlighting the moderate reactivity of the designed α-chloroacetamides. The remaining *covalentizer* hits included a 2.01 µM inhibitor (**3**) of FGFR4 derived from the non-selective kinase inhibitor ponatinib, and a 155 nM inhibitor (**4**) of GSK3β.

A covalent SARS-CoV-2 main protease inhibitor

Upon the release of the first structure of the new SARS-CoV-2 M^pro protease (PDB: 6LU7[44]) we noticed that the active site is nearly identical to that of SARS-CoV-1. The entire protein is highly conserved with 96% sequence identity. This prompted us to search the database for covalent versions of SARS-CoV-1 M^pro ligands. One such prediction was available based on a reversible inhibitor ML188 (IC_{50}= 4.8 ± 0.8 µM, racemate; 1.5 ± 0.3 µM, (*R*)-enantiomer) of the SARS-CoV-1 main protease (PDB: 3V3M[37]; Fig. 5A). We re-synthesized and tested racemic ML188 against SARS-CoV-2 M^pro which showed an IC_{50} of 3.14 µM (Supp. Fig. 4A), similar to what has been reported for SARS-CoV-1. ML188 was synthesized using the Ugi four-component

287   reaction (4-CR), and the covalent prediction was easily accessible by replacing one reactant (2-
288   furoic acid to acrylic acid) to give **10**, synthesized and isolated as the racemate (Fig. 5D). We
289   initially assessed irreversible binding of **10** towards recombinant SARS-CoV-2 M^{pro} using intact
290   protein mass spectrometry (2 μM protein, 1.5 h incubation with electrophile at 25 °C; Fig. 5F).
291   The expected adduct was detected with 19% labeling at 2 μM compound, and up to 88% labeling
292   at 200 μM compound (Fig. 5F).

293   Despite the irreversible binding, this initial compound did not show strong inhibition in a
294   fluorescence-based enzymatic assay ($IC_{50} > 99$ μM, 13% inhibition at 20 μM; 15 min pre-
295   incubation; Fig. 5H). However, it was a promising starting point for additional optimization. Due
296   to the modular nature of the Ugi 4-CR procedure, it was possible to synthesize and test large
297   libraries of analogs by systematically varying each reactant to target different pockets. We
298   designed those libraries based on computational modelling of *in silico* generated Ugi products, as
299   well as an exhaustive screen of commercially available isocyanides (see Supp. Dataset 1). A few
300   of the early combinatorial synthetic results, which had low biochemical potency (comparable to
301   our starting Ugi compound), allowed for crystallographic analysis in the presence of M^{pro}. In these
302   cases, the expected binding mode was recapitulated experimentally and showed low deviation
303   from the non-covalent starting point (Fig. 5B, 5C, Supp. Fig. 5), thus proving the *covalentizer*
304   prediction to be correct. In all crystal structures, the electrophile formed the expected covalent
305   bond with the catalytic cysteine residue.

306   To optimize **10**, we have made and tested close to 140 analogs (Supp. Dataset 1; Fig. 5.
307   Supp. Fig. 7,8), exploring all three components of the Ugi reaction while keeping the acrylamide
308   fixed. We explored a variety of replacements for the initial *p-tert*-butylphenyl motif protruding
309   into the S2 pocket (Fig. 5), most of them did not result in improved potency (Supp. Fig. 7C).
310   Similarly, independent optimization of binding to the S1 pocket only led to the identification of
311   one beneficial change (**23**, IC_{50} 65.58 μM), with a *meta* chloro-substitution of the pyridine (Supp.
312   Fig. 7A). Other substituents (-Br, -OMe, -OEt, $-CF_2CH_3$) led to inactive compounds.

313   Beyond further optimization of the S1 and S2 pocket binding it was clear that extension of
314   the ligand towards the S3 and S4 pockets should prove fruitful. For example, a reversible-covalent
315   α-ketoamide inhibitor[46] (biochemical IC_{50} 0.67 μM ± 0.18 μM) probes the S3/4 region with an
316   additional hydrogen bond to the backbone of Glu166. In a large scale fragment screen, numerous
317   fragments were able to bind in these pockets[47]. In this case, we exhaustively synthesized analogs
318   of **10**, using 34 available isocyanides. Starting from **10**, simple alkyl chain extension resulted in
319   compounds with improved potency (Fig. 5D). In particular compound **11**, harboring a
320   phenethylamide motif, was particularly potent with an IC_{50} of 2.95 μM (Fig. 5G) and K_{inact}/K_i of
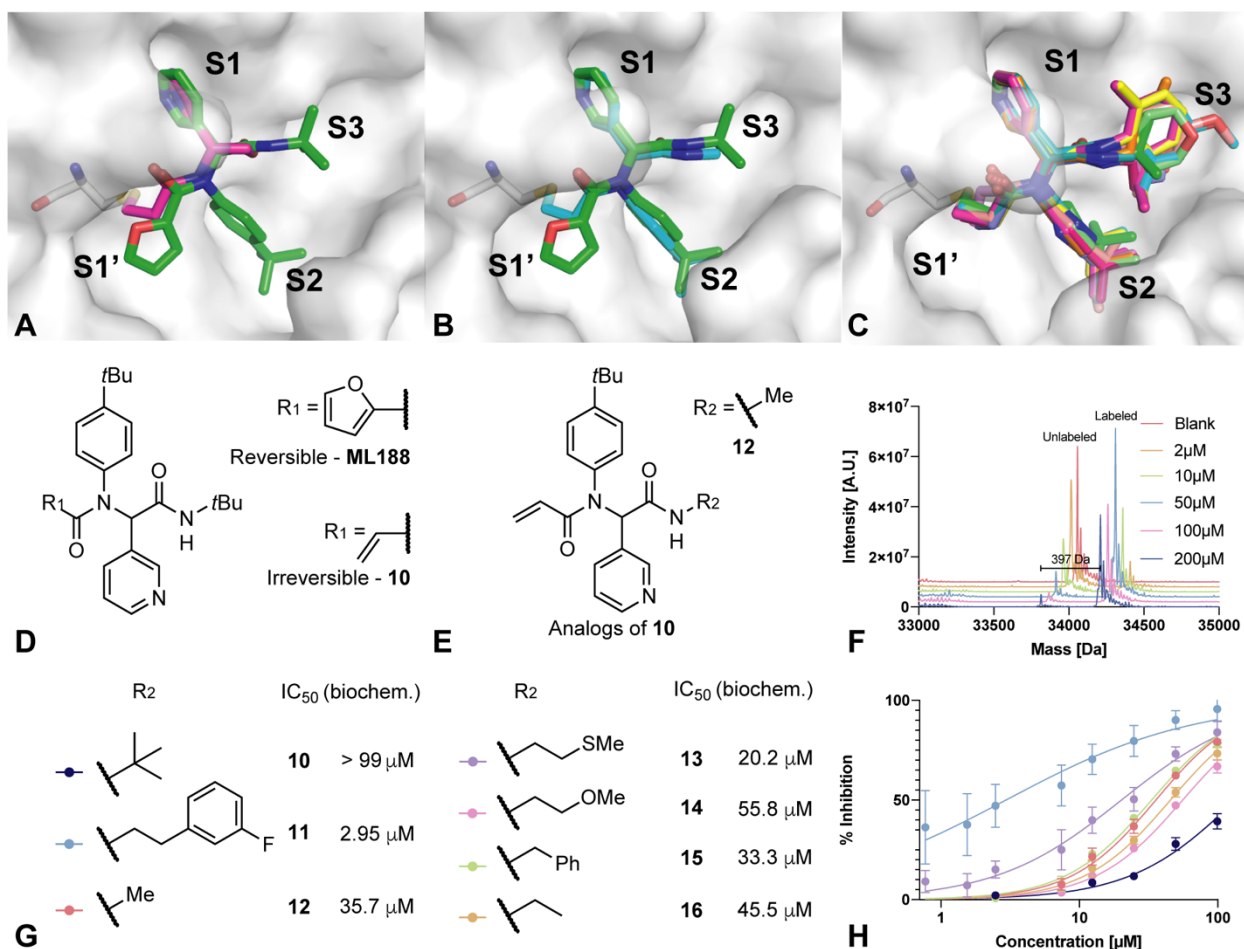321   18.4 $M^{-1}s^{-1}$ (Supp. Fig. 6).

322

Figure 5. Computational prediction and experimental validation of an irreversible SARS-CoV-2 M^{pro} inhibitor.
A. The *covalentizer* prediction of **10** (magenta) overlaid on the non-covalent compound it is based on (ML188[45]; green; PDB:3V3M). The protocol suggested to substitute the furanyl moiety of ML188 with an acrylamide to bind the catalytic cysteine. The RMSD between the covalent fragment and the original reversible inhibitor is 0.65 Å. **B.** The crystal structure of one of the covalent analogs of **10** (PDB: 5RH5; cyan) overlaid on ML188 (green). **C.** Overlay of all the 11 crystal structures of compound **10** analogs, all exhibiting the same predicted binding mode. PDBs: 5RGT, 5RH5, 5RH6, 5RH7, 5RH9, 5RL0, 5RL1, 5RL2, 5RL3, 5RL4, 5RL5. For individual structures see Supp. Fig. 5. **D.** The chemical structures of ML188 and **10**. **E.** Chemical structure of Ugi compounds exploring the S3 pocket, with the R group that is shown in the crystal structure in (B). **F.** Deconvoluted mass spectra obtained by intact protein LC/MS of recombinant SARS-CoV-2 M^{pro} 2μM incubated with 2 μM - 200 μM **10** for 1.5 h at room temperature. **G.** Further analogs of **10** with their associated biochemical potencies. **H.** The dose response curves for the seven compounds shown in G.

It appears that relief of steric strain around the amide nitrogen also plays a part, since change to a methyl amide (in **12**, relative to **10**) also resulted in increased potency. Opposed to our initial assumption of independent optimization of S1-3 pocket binding, the combination of beneficial structural motifs in a third generation of Ugi products led to inhibitors with diminished potency compared to **11** (see Supp. Fig. 7B; Supp. Dataset 1). One explanation for this behaviour is the high plasticity of M^{pro}, leading to induced fit effects.

343   Removal of the furanyl in ML188 and replacement with an electrophile in **10** initially led
344   to a loss in potency, which in this case was overcome by optimization of the non-covalent affinity
345   in the S3 region to give compound **11**. Re-installing the furanyl ring in combination with the S3-
346   optimized phenethylamide motif led to compound **17** with a similar IC_{50} (2.72. μM; Supp. Fig.
347   4B), suggesting that the marked improvement of this side-chain is particular to the covalently
348   bound conformation.

349   In conclusion, we successfully executed a mode of action change towards irreversible
350   targeting of the catalytic cysteine residue in M^{pro} which may have improved activity in cells as
351   well as long-term strategic benefits to safeguard against viral evolution.

352

Discussion

Designing new covalent inhibitors is challenging. Here we leveraged the subset of protein targets for which a structure of a known binder is available, to computationally enumerate and evaluate exhaustive sets of covalent derivatives. Automating the protocol allowed us to apply it to the entire PDB and assess the applicability of this approach. Prospective testing against six real-world targets demonstrated that irreversible ligands can be reached with little synthesis, and structures validated the binding-pose prediction.

A main advantage of our work is the wide exploration of X-ray structures which produced an extensive list of candidates waiting to be explored. This allowed us to quickly find a promising lead series against SARS-CoV-2 M^{pro}. This prediction, which was based on a historic non-covalent SARS-CoV-1 M^{pro} inhibitor[45] was pre-calculated, and ready for synthesis at a moment's notice. We have made thousands of such predictions available through a public website (https://covalentizer.weizmann.ac.il) which updates weekly with the release of new structures to the PDB. It also allows *covalentizing* of user uploaded structures. We believe this would enable wide application and experimental testing of new covalent inhibitors.

Despite the success of our protocol, several caveats remain. First is the fact that currently the protocol does not take into account the synthetic feasibility of the proposed designs. When selecting candidates for prospective evaluation, we found that some of the molecules required complicated synthesis. Incorporating into our pipeline a strategy such as DOTS[33,48], other retrosynthesis algorithms[49–51] or even the use of synthetic feasibility scores[52–54], can significantly improve the quality of proposed candidates in the future.

Another point for improvement is the relatively weak potency of our prospective designs in comparison to their parent compounds. One likely explanation for these lower affinities is the removal of non-covalent affinity elements which are not sufficiently compensated by the gains from covalent bond formation. For example, in compound **2** (derived from PDB: 4QTA) more than 350 Da of the original compound[55] is removed (Supp. Fig. 2), resulting in three orders of magnitude loss in potency. However the remaining covalent fragment still shows significant inhibition of ERK2. Another example is compound **1**, its parent compound (PDB: 4QP9) has an IC$_{50}$ of 71 nM, however the propyl-pyrazole group we have omitted in order to accommodate the electrophile (Supp. Fig. 2) improved the parent reversible binder by more than 150-fold. Lastly the loss of a hydrogen bond between the M^{pro} backbone NH of Gly143 and the furanyl oxygen of ML188 (PDB: 3V3M), decreased potency, under our assay conditions of 15 min. pre-incubation, by more than 30-fold. These results suggest that a careful examination of the binding energy contribution is required for the parts that are omitted in order to accommodate the new electrophile.

392   However, as we saw for both ERK2 (**1** *vs.* **5**) and M[pro] (**10** *vs.* **11**), improving reversible
393   recognition is able to improve potency, and even to surpass the parent compound in the case of **11**.
394   For this series we believe that further structure-based optimization of binding to the S3 pocket,
395   including H-bonding to Glu166 and chiral separation of the active enantiomer can pave the way
396   for sub-micromolar Ugi-type covalent M[pro] inhibitors. Thus, in many cases where irreversible
397   binding is needed our protocol can provide a promising starting point for optimization.
398
399   Another possible explanation for the relatively low affinity of the irreversible binders are
400   slight inaccuracies in the covalent warhead positioning which results in sub-optimal covalent bond
401   formation. Perhaps due to the fact that the docking program does not take into account the actual
402   formation of the covalent bond, and ignores for instance the transition state energy of the rate-
403   determining step of the organosulfide bond formation, but rather evaluates the binding energy of
404   the adduct. Better understanding of the steric and electronic constraints of the covalent bond
405   formation, and hence a better docking software should improve the results.
406
407   The docking software also ignores the intrinsic reactivity of the proposed designs. It is
408   interesting to note in this regard the similar activity of a methylene-chloroacetamide (**1**), compared
409   to its acrylamide analog (**6**). Such electrophile replacements can be very useful in rational design
410   of irreversible inhibitors, especially if they prove to work across various scaffolds. Geometrically,
411   the additional methylene before the chloroacetamide makes the distance from the ring to the thiol
412   similar to that of the acrylamide (Supp. Fig. 2). In terms of reactivity, however, the acrylamide,
413   conjugated to the azaindole is activated[56] and thus is likely closer in reactivity to the
414   chloroacetamide. Indeed, a methylene linker would be the minimal linker element required to
415   insulate against π-conjugation, allowing easier prediction of intrinsic reactivity. No-linker designs
416   connected to extended π-systems such as heteroarenes often exhibit a range of intrinsic
417   reactivities[20,56] which remain challenging to predict computationally[57–59] and thus require careful
418   evaluation.
419
420   Many additional designs remain to be discovered beyond the more than 1,500 we made
421   available through the *covalentizer* server. New electrophiles and linkers which will enable new
422   geometric trajectories between the cysteine and the molecule, can considerably expand the design
423   space. We tested this idea computationally using a library of linkers curated from the literature
424   (Supp. Fig 1), on a subset of kinases from our database, showing an increase in the number of
425   structures that can be *covalentized*. New covalent 'warheads', including reversible covalent
426   warheads, such as cyanoacrylamides[60], and clorofluoroacetamides[61] become available, both for
427   cysteine residues[62], but also for other amino acids[63–65]. These can be incorporated with little effort
428   into the *covalentizer* pipeline. Since cysteine is one of the least abundant natural amino acids,
429   additional covalent chemistries will significantly expand the number of ligands that can be
430   potentially addressed.
431

432   In summary, we show that using covalent docking we were able to make irreversible
433   analogs of ligands for which a complex structure is available. We made our discoveries public in
434   the form of a database of the results we obtained by running our protocol on the entire PDB which
435   is automatically updated weekly with newly released entries, as well as a web-tool for applying
436   the protocol on new targets given by users. Using the protocol, we discovered new covalent kinase
437   inhibitors and optimised a potent covalent COVID-19 protease inhibitor, with a low-cost, modular
438   and fast synthesis. We hope our results will encourage researchers to apply covalent inhibitors for
439   a wide range of targets.
440

Methods

Programs and libraries

RDKit was used for 2D molecular handling, conformation generation and RMSD calculation. RDKit: Open-source cheminformatics; RDKit.org. Marvin was used in the process of preparing the molecules for docking, Marvin 17.21.0, ChemAxon (https://www.chemaxon.com). DOCKovalent [26] was used for virtual covalent docking.

Curating target structures from the PDB

Using pymol scripts (The PyMOL Molecular Graphics System, Version 2.0.4 Schrödinger, LLC), we filtered only the structures that have a ligand in which one of its atoms is within 6 Å cysteine residue. We further filtered the list to include only cysteines with a free thiol group (defined as a sulfur atom that is only connected to the residue's Cβ). By doing this, we discarded any disulfides, as well as cysteines that are already covalently attached to a ligand. We further removed any ligands which had more than one copy per chain in the structure, and ligands on which processing of the ligand's SMILES failed.

Enumerating substructures for covalentization

Fragmentation and scaffold extraction was done using RDKit's implementation of the Recap algorithm [38] and the MurckoScaffold [39] functionality respectively.

Covalentizing a substructure

For each substructure or scaffold, we generated a library of potential electrophilic analogs using SMARTS based reactions. The reaction rules were: 1. Adding an electrophile (including the nitrogen) to any non-substituted aromatic carbon, as well as all aliphatic carbons with one or two bonded atoms, excluding carbons which are already connected to nitrogen. 2. Adding an electrophile to a free amine, either primary or secondary. In this case the nitrogen is completed with the rest of the electrophile. The first rule will usually require more complicated synthesis, whereas the second rule, will allow to use the same ligand as a starting material for a nucleophilic substitution of the acyl form of the electrophile with the free amine.

Docking and RMSD calculation

RDKit and Marvin were used to create 250 conformations for each electrophilic analog. Covalent docking was done using DOCKovalent – a virtual screening program. We docked the appropriate analog library for each target, while saving 10 structures for each analog to increase the number of final candidates. When docking the larger linker based libraries we only used the top scoring structure for each analog, due to the large number of structures for analysis. Alternative rotamers for the cysteine residue were generated with pymol based scripts. We used RDKit to filter only for results with a MCS that has an RMSD of less than 1.5 Å to the original ligand.

Computational optimisation of the M^{pro} inhibitor

We used the RDKit reaction functionalities, as well as OpenBabel (http://openbabel.org/wiki/Main_Page) to prepare virtual libraries of analogs of compound **10**. The Ugi reaction has three reactants: amine, isocyanide, aldehyde and carboxylic acid. The carboxylic acid is set constant to acrylic acid, since we didn't want to change the electrophilic component. In the virtual libraries, we left it as the reversible furan moiety for convenience in modeling. We thus created three such libraries, each one by replacing one of the three other Ugi reactants with commercially available building blocks. Using RDKit, we generated up to 100 constrained conformations of each molecule, by fixing the conformation of three components as in the crystal structure, and changing only the conformation of the variable part. We then used the Rosetta modeling suite in order to choose the best conformation for each compound, when bound to the protease. For each molecule, we then defined this set of constrained conformations as an extra residue for Rosetta, and used Rosetta Packer[66] to choose the best conformation, while allowing side-chain flexibility. Eventually, we chose analogs only for the amine and the isocyanide components, as the aldehyde component was highly optimised already. We chose 9 isocyanide replacements and 14 amine replacements (one of them was not based on docking). Most combinations of these components were made by Enamine and tested as part of the Covid-Moonshot effort[47,67].

Intact protein LC/MS

M^{pro} was incubated for 90 minutes in 50 mM Tris pH 8 300 mM NaCl in room temperature. ERK2 was incubated for 60 minutes in 10 mM Hepes pH 7.5 500 mM NaCl and 5% glycerol in room temperature. The LC/MS runs were performed on a Waters ACUITY UPLC class H instrument, in positive ion mode using electrospray ionization. UPLC separation used a C4 column (300 Å, 1.7 μm, 21 mm × 100 mm). The column was held at 40 °C and the autosampler at 10 °C. Mobile solution A was 0.1% formic acid in water, and mobile phase B was 0.1% formic acid in acetonitrile. The run flow was 0.4 mL/min with gradient 20% B for 4 min, increasing linearly to 60% B for 2 min, holding at 60% B for 0.5 min, changing to 0% B in 0.5 min, and holding at 0% for 1 min. The mass data were collected on a Waters SQD2 detector with an m/z range of 2−3071.98 at a range of 1000−2000 m/z. The mass data were collected on a Waters SQD2 detector with an m/z range of 2–3071.98 at a range of 900–1500 m/z for ERK2 and 1000–2000 m/z for M^{pro}. The desolvation temperature was 500 °C with a flow rate of 1000 L/h. The voltages used were 0.69 kV for the capillary and 46 V for the cone. Raw data were processed using openLYNX and deconvoluted using MaxEnt (20 - 60 kDa window, 1 Da/channel resolution)**.**

Kinase activity assays

Biochemical Kinase inhibition assays were carried out at Nanosyn, Santa Clara. Test compounds were diluted in 100% DMSO using 3-fold dilution steps. Final compound concentration in assay ranged from 10 μM to 0.0565 nM. Compounds were tested in a single well for each dilution, and the final concentration of DMSO in all assays was kept at 1%. Reference

521 compound, Staurosporine, was tested in an identical manner. Compounds were preincubated in
522 25C for 2 hours before the measurements, and the kinase reactions were then performed for an
523 additional 3 hours. For ERK2, the kinase concentration was 0.25-0.35 nM, the ATP concentration
524 was 25 µM. For MELK, the kinase concentration was 0.06 nM, the ATP concentration was 30
525 µM. For VEGFR2, the kinase concentration was 0.25 nM, the ATP concentration was 80 µM. For
526 GSK3B, the kinase concentration was 0.09 nM, the ATP concentration was 10 µM. For FGFR4,
527 the kinase concentration was 0.17 nM, the ATP concentration was 250 µM.
528
529 *Biochemical M^{pro} inhibition assay*
530   Compounds were seeded into assay-ready plates (Greiner 384 low volume 784900) using
531 an Echo 555 acoustic dispenser, and DMSO was back-filled for a uniform concentration in assay
532 plates (maximum 1%). Reagents for M^{pro} assay were dispensed into the assay plate in 10 µl
533 volumes for a final of 20 µl. Final reaction concentrations were 20 mM HEPES pH=7.3, 1mM
534 TCEP, 50 mM NaCl, 0.01% Tween-20, 10% glycerol, 5 nM M^{pro}, 375 nM fluorogenic peptide
535 substrate ([5-FAM]-AVLQSGFR-[Lys(Dabcyl)]-K-amide). M^{pro} was pre-incubated for 15
536 minutes at room temperature with compound before addition of substrate. Protease reaction was
537 measured continuously in a BMG Pherastar FS with a 480/520 ex/em filter set. Data was mapped
538 and normalized in Genedata Screener.
539
540 *M^{pro}*   *Crystallography*
541   M^{pro} protein was expressed and purified as discussed previously[47]. Apo M^{pro} crystals were
542 grown using the sitting drop vapour diffusion method at 20 °C by adding 150 nl of protein (5
543 mg/ml in 20 mM Hepes pH 7.5, 50 mM NaCl) to 300 nl of crystallisation solution (11% PEG 4K,
544 6% DMSO, 0.1M MES pH 6.7) and 50 nl of seed stock prepared from initial crystal hits. 55 nl of
545 a 100 mM compound stock solution in DMSO was added directly to the crystallisation drops using
546 an ECHO liquid handler (final concentration 10% DMSO) and drops were incubated for
547 approximately 1 hour prior to mounting and flash freezing in liquid nitrogen. Data were collected
548 at Diamond Light Source on beamline I04-1 at 100K and processed using XDS[68] and either xia2[69],
549 autoPROC[70] or DIALS[71]. Further analysis was performed with XChemExplorer[72]: electron
550 density maps were generated with Dimple[73]; ligand-binding events were identified using
551 PanDDA[74] (both the released version 0.2 and the pre-release development version
552 (https://github.com/ConorFWild/pandda)); ligands were modelled into PanDDA-calculated event
553 maps using Coot[75]; restraints were calculated with GRADE[76]; and structures were refined with
554 BUSTER[77]. Coordinates, structure factors and PanDDA event maps for all data sets are deposited
555 in the Protein Data Bank under PDB IDs 5RGT, 5RH5, 5RH6, 5RH7, 5RH9, 5RL0, 5RL1, 5RL2,
556 5RL3, 5RL4 and 5RL5. Data collection and refinement statistics are summarised in Supplementary
557 Table 2. The ground-state structure and all corresponding datasets are deposited under PDB ID
558 5R8T.
559
560

References

1. Burger, J. A. & Buggy, J. J. Bruton tyrosine kinase inhibitor ibrutinib (PCI-32765). *Leukemia & Lymphoma* vol. 54 2385–2391 (2013).

2. Sequist, L. V. *et al.* Phase III study of afatinib or cisplatin plus pemetrexed in patients with metastatic lung adenocarcinoma with EGFR mutations. *J. Clin. Oncol.* **31**, 3327–3334 (2013).

3. Oxnard, G. R. *et al.* Association Between Plasma Genotyping and Outcomes of Treatment With Osimertinib (AZD9291) in Advanced Non-Small-Cell Lung Cancer. *J. Clin. Oncol.* **34**, 3375–3382 (2016).

4. Bradshaw, J. M. *et al.* Prolonged and tunable residence time using reversible covalent kinase inhibitors. *Nat. Chem. Biol.* **11**, 525–531 (2015).

5. Lonsdale, R. & Ward, R. A. Structure-based design of targeted covalent inhibitors. *Chem. Soc. Rev.* **47**, 3816–3830 (2018).

6. Michalczyk, A. *et al.* Structural insights into how irreversible inhibitors can overcome drug resistance in EGFR. *Bioorg. Med. Chem.* **16**, 3482–3488 (2008).

7. Yun, C.-H. *et al.* The T790M mutation in EGFR kinase causes drug resistance by increasing the affinity for ATP. *Proc. Natl. Acad. Sci. U. S. A.* **105**, 2070–2075 (2008).

8. Ghosh, A. K., Samanta, I., Mondal, A. & Liu, W. R. Covalent Inhibition in Drug Discovery. *ChemMedChem* **14**, 889–906 (2019).

9. Cohen, M. S., Zhang, C., Shokat, K. M. & Taunton, J. Structural bioinformatics-based design of selective, irreversible kinase inhibitors. *Science* **308**, 1318–1321 (2005).

10. Nnadi, C. I. *et al.* Novel K-Ras G12C Switch-II Covalent Binders Destabilize Ras and Accelerate Nucleotide Exchange. *J. Chem. Inf. Model.* **58**, 464–471 (2018).

11. Zeng, M. *et al.* Potent and Selective Covalent Quinazoline Inhibitors of KRAS G12C. *Cell Chem Biol* **24**, 1005–1016.e3 (2017).

12. Canon, J. *et al.* The clinical KRAS(G12C) inhibitor AMG 510 drives anti-tumour immunity. *Nature* **575**, 217–223 (2019).

13. Vazquez-Rodriguez, S. & Wright, M. Design, Synthesis and Characterization of Covalent KDM5 Inhibitors. *Angewandte* (2019).

14. Dubiella, C., Baur, R., Cui, H., Huber, E. M. & Groll, M. Selective Inhibition of the Immunoproteasome by Structure-Based Targeting of a Non-catalytic Cysteine. *Angew. Chem. Int. Ed.* **54**, 15888–15891 (2015).

15. Angst, D. *et al.* Discovery of LOU064 (Remibrutinib), a Potent and Highly Selective Covalent Inhibitor of Bruton's Tyrosine Kinase. *J. Med. Chem.* **63**, 5102–5118 (2020).

16. Weisner, J. *et al.* Covalent-allosteric kinase inhibitors. *Angew. Chem. Int. Ed.* **54**, 10313–10316 (2015).

17. Hagel, M. *et al.* First Selective Small Molecule Inhibitor of FGFR4 for the Treatment of Hepatocellular Carcinomas with an Activated FGFR4 Signaling Pathway. *Cancer Discov.* **5**, 424–437 (2015).

18. Ward, R. A. *et al.* Structure-Guided Design of Highly Selective and Potent Covalent Inhibitors of ERK1/2. *J. Med. Chem.* **58**, 4790–4801 (2015).

19. Backus, K. M. *et al.* Proteome-wide covalent ligand discovery in native biological systems. *Nature* **534**, 570–574 (2016).

20. Resnick, E. *et al.* Rapid Covalent-Probe Discovery by Electrophile-Fragment Screening. *J. Am. Chem. Soc.* **141**, 8951–8968 (2019).

606   21. Johansson, H. *et al.* Fragment-Based Covalent Ligand Screening Enables Rapid Discovery
607   of Inhibitors for the RBR E3 Ubiquitin Ligase HOIP. *J. Am. Chem. Soc.* **141**, 2703–2712
608   (2019).
609   22. Kathman, S. G., Xu, Z. & Statsyuk, A. V. A fragment-based method to discover irreversible
610   covalent inhibitors of cysteine proteases. *J. Med. Chem.* **57**, 4969–4974 (2014).
611   23. Kathman, S. G. *et al.* A Small Molecule That Switches a Ubiquitin Ligase From a
612   Processive to a Distributive Enzymatic Mechanism. *J. Am. Chem. Soc.* **137**, 12442–12445
613   (2015).
614   24. Craven, G. B. *et al.* High-Throughput Kinetic Analysis for Target-Directed Covalent
615   Ligand Discovery. *Angew. Chem. Int. Ed Engl.* **57**, 5257–5261 (2018).
616   25. Parker, C. G. *et al.* Ligand and Target Discovery by Fragment-Based Screening in Human
617   Cells. *Cell* **168**, 527–541.e29 (2017).
618   26. London, N. *et al.* Covalent docking of large libraries for the discovery of chemical probes.
619   *Nat. Chem. Biol.* **10**, 1066–1072 (2014).
620   27. Shraga, A. *et al.* Covalent Docking Identifies a Potent and Selective MKK7 Inhibitor. *Cell
621   Chem Biol* **26**, 98–108.e5 (2019).
622   28. Toledo Warshaviak, D., Golan, G., Borrelli, K. W., Zhu, K. & Kalid, O. Structure-based
623   virtual screening approach for discovery of covalently bound ligands. *J. Chem. Inf. Model.*
624   **54**, 1941–1950 (2014).
625   29. Rachman, M. *et al.* DUckCov: a Dynamic Undocking-Based Virtual Screening Protocol for
626   Covalent Binders. *ChemMedChem* **14**, 1011–1021 (2019).
627   30. Scarpino, A., Ferenczy, G. G. & Keserű, G. M. Comparative Evaluation of Covalent
628   Docking Tools. *Journal of Chemical Information and Modeling* vol. 58 1441–1458 (2018).
629   31. Bensinger, D. *et al.* Virtual Screening Identifies Irreversible FMS-like Tyrosine Kinase 3
630   Inhibitors with Activity toward Resistance-Conferring Mutations. *J. Med. Chem.* **62**, 2428–
631   2446 (2019).
632   32. Chowdhury, S. R. *et al.* Discovery of covalent enzyme inhibitors using virtual docking of
633   covalent fragments. *Bioorg. Med. Chem. Lett.* **29**, 36–39 (2019).
634   33. Hoffer, L. *et al.* CovaDOTS: In Silico Chemistry-Driven Tool to Design Covalent Inhibitors
635   Using a Linking Strategy. *J. Chem. Inf. Model.* **59**, 1472–1485 (2019).
636   34. Wei, L. *et al.* Cov_FB3D: A De Novo Covalent Drug Design Protocol Integrating the BA-
637   SAMP Strategy and Machine-Learning-Based Synthetic Tractability Evaluation. *J. Chem.
638   Inf. Model.* (2020) doi:10.1021/acs.jcim.9b01197.
639   35. Zhu, N. *et al.* A Novel Coronavirus from Patients with Pneumonia in China, 2019. *N. Engl.
640   J. Med.* **382**, 727–733 (2020).
641   36. Wu, F. *et al.* A new coronavirus associated with human respiratory disease in China. *Nature*
642   **579**, 265–269 (2020).
643   37. Jacobs, J. *et al.* Discovery, Synthesis, And Structure-Based Optimization of a Series ofN-
644   (tert-Butyl)-2-(N-arylamido)-2-(pyridin-3-yl) Acetamides (ML188) as Potent Noncovalent
645   Small Molecule Inhibitors of the Severe Acute Respiratory Syndrome Coronavirus (SARS-
646   CoV) 3CL Protease. *Journal of Medicinal Chemistry* vol. 56 534–546 (2013).
647   38. Lewell, X. Q., Judd, D. B., Watson, S. P. & Hann, M. M. RECAP--retrosynthetic
648   combinatorial analysis procedure: a powerful new technique for identifying privileged
649   molecular fragments with useful applications in combinatorial chemistry. *J. Chem. Inf.
650   Comput. Sci.* **38**, 511–522 (1998).
651   39. Bemis, G. W. & Murcko, M. A. The properties of known drugs. 1. Molecular frameworks.

J. Med. Chem. **39**, 2887–2893 (1996).

40. Shi, L., Zhong, Z., Li, X., Zhou, Y. & Pan, Z. Discovery of an Orally Available Janus Kinase 3 Selective Covalent Inhibitor. *J. Med. Chem.* **62**, 1054–1066 (2019).

41. Caldwell, R. D. *et al.* Discovery of Evobrutinib: An Oral, Potent, and Highly Selective, Covalent Bruton's Tyrosine Kinase (BTK) Inhibitor for the Treatment of Immunological Diseases. *J. Med. Chem.* **62**, 7643–7655 (2019).

42. Liang, X. *et al.* Discovery of 2-((3-Acrylamido-4-methylphenyl)amino)-N-(2-methyl-5-(3,4,5-trimethoxybenzamido)phenyl)-4-(methylamino)pyrimidine-5-carboxamide (CHMFL-BMX-078) as a Highly Potent and Selective Type II Irreversible Bone Marrow Kinase in the X Chromosome (BMX) Kinase Inhibitor. *J. Med. Chem.* **60**, 1793–1816 (2017).

43. Engel, J. *et al.* Targeting Drug Resistance in EGFR with Covalent Inhibitors: A Structure-Based Design Approach. *J. Med. Chem.* **58**, 6844–6863 (2015).

44. Jin, Z. *et al.* Structure of Mpro from COVID-19 virus and discovery of its inhibitors. *bioRxiv* (2020).

45. Jacobs, J. *et al.* Discovery, synthesis, and structure-based optimization of a series of N-(tert-butyl)-2-(N-arylamido)-2-(pyridin-3-yl) acetamides (ML188) as potent noncovalent small molecule inhibitors of the severe acute respiratory syndrome coronavirus (SARS-CoV) 3CL protease. *J. Med. Chem.* **56**, 534–546 (2013).

46. Zhang, L. *et al.* Crystal structure of SARS-CoV-2 main protease provides a basis for design of improved α-ketoamide inhibitors. *Science* (2020) doi:10.1126/science.abb3405.

47. Douangamath, A. *et al.* Crystallographic and electrophilic fragment screening of the SARS-CoV-2 main protease. *bioRxiv* 2020.05.27.118117 (2020) doi:10.1101/2020.05.27.118117.

48. Hoffer, L. *et al.* Integrated Strategy for Lead Optimization Based on Fragment Growing: The Diversity-Oriented-Target-Focused-Synthesis Approach. *J. Med. Chem.* **61**, 5719–5732 (2018).

49. Delépine, B., Duigou, T., Carbonell, P. & Faulon, J.-L. RetroPath2.0: A retrosynthesis workflow for metabolic engineers. *Metab. Eng.* **45**, 158–170 (2018).

50. Law, J. *et al.* Route Designer: a retrosynthetic analysis tool utilizing automated retrosynthetic rule generation. *J. Chem. Inf. Model.* **49**, 593–602 (2009).

51. Watson, I. A., Wang, J. & Nicolaou, C. A. A retrosynthetic analysis algorithm implementation. *J. Cheminform.* **11**, 1 (2019).

52. Ertl, P. & Schuffenhauer, A. Estimation of synthetic accessibility score of drug-like molecules based on molecular complexity and fragment contributions. *J. Cheminform.* **1**, 8 (2009).

53. Huang, Q., Li, L.-L. & Yang, S.-Y. RASA: a rapid retrosynthesis-based scoring method for the assessment of synthetic accessibility of drug-like molecules. *J. Chem. Inf. Model.* **51**, 2768–2777 (2011).

54. Podolyan, Y., Walters, M. A. & Karypis, G. Assessing synthetic accessibility of chemical compounds using machine learning methods. *J. Chem. Inf. Model.* **50**, 979–991 (2010).

55. Chaikuad, A. *et al.* A unique inhibitor binding site in ERK1/2 is associated with slow binding kinetics. *Nat. Chem. Biol.* **10**, 853–860 (2014).

56. Flanagan, M. E. *et al.* Chemical and computational methods for the characterization of covalent reactive groups for the prospective design of irreversible inhibitors. *J. Med. Chem.* **57**, 10072–10079 (2014).

57. Palazzesi, F. *et al.* BIreactive: A Machine-Learning Model to Estimate Covalent Warhead

698   Reactivity. *J. Chem. Inf. Model.* **60**, 2915–2923 (2020).

699 58. Palazzesi, F., Grundl, M. A., Pautsch, A., Weber, A. & Tautermann, C. S. A Fast Ab Initio
700   Predictor Tool for Covalent Reactivity Estimation of Acrylamides. *J. Chem. Inf. Model.*
701   (2019) doi:10.1021/acs.jcim.9b00316.

702 59. Lonsdale, R. *et al.* Expanding the Armory: Predicting and Tuning Covalent Warhead
703   Reactivity. *J. Chem. Inf. Model.* **57**, 3124–3137 (2017).

704 60. Bandyopadhyay, A. & Gao, J. Targeting biomolecules with reversible covalent chemistry.
705   *Curr. Opin. Chem. Biol.* **34**, 110–116 (2016).

706 61. Shindo, N. *et al.* Selective and reversible modification of kinase cysteines with
707   chlorofluoroacetamides. *Nat. Chem. Biol.* **15**, 250–258 (2019).

708 62. Backus, K. M. Applications of Reactive Cysteine Profiling. *Curr. Top. Microbiol. Immunol.*
709   **420**, 375–417 (2019).

710 63. Martín-Gago, P. & Olsen, C. A. Arylfluorosulfate-Based Electrophiles for Covalent Protein
711   Labeling: A New Addition to the Arsenal. *Angew. Chem. Int. Ed.* **58**, 957–966 (2019).

712 64. Shannon, D. A. & Weerapana, E. Covalent protein modification: the current landscape of
713   residue-specific electrophiles. *Curr. Opin. Chem. Biol.* **24**, 18–26 (2015).

714 65. Ray, S. & Murkin, A. S. New Electrophiles and Strategies for Mechanism-Based and
715   Targeted Covalent Inhibitor Design. *Biochemistry* (2019)
716   doi:10.1021/acs.biochem.9b00293.

717 66. Kuhlman, B. & Baker, D. Native protein sequences are close to optimal for their structures.
718   *Proc. Natl. Acad. Sci. U. S. A.* **97**, 10383–10388 (2000).

719 67. Chodera, J., Lee, A. A., London, N. & von Delft, F. Crowdsourcing drug discovery for
720   pandemics. *Nat. Chem.* **12**, 581 (2020).

721 68. Kabsch, W. Integration, scaling, space-group assignment and post-refinement. *Acta*
722   *Crystallographica Section D Biological Crystallography* vol. 66 133–144 (2010).

723 69. Winter, G., Lobley, C. M. C. & Prince, S. M. Decision making in xia2. *Acta Crystallogr. D*
724   *Biol. Crystallogr.* **69**, 1260–1273 (2013).

725 70. Vonrhein, C. *et al.* Data processing and analysis with the autoPROC toolbox. *Acta*
726   *Crystallogr. D Biol. Crystallogr.* **67**, 293–302 (2011).

727 71. Winter, G. *et al.* DIALS: implementation and evaluation of a new integration package. *Acta*
728   *Crystallogr D Struct Biol* **74**, 85–97 (2018).

729 72. Krojer, T. *et al.* The XChemExplorer graphical workflow tool for routine or large-scale
730   protein–ligand structure determination. *Acta Crystallographica Section D: Structural*
731   *Biology* **73**, 267–278 (2017).

732 73. Keegan, R., Wojdyr, M., Winter, G. & Ashton, A. DIMPLE: a difference map pipeline for
733   the rapid screening of crystals on the beamline. in *Acta Crystallographica a-Foundation*
734   *and Advances* vol. 71 S18–S18 (INT UNION CRYSTALLOGRAPHY 2 ABBEY SQ,
735   CHESTER, CH1 2HU, ENGLAND, 2015).

736 74. Pearce, N. M. *et al.* A multi-crystal method for extracting obscured crystallographic states
737   from conventionally uninterpretable electron density. *Nat. Commun.* **8**, 15123 (2017).

738 75. Emsley, P., Lohkamp, B., Scott, W. G. & Cowtan, K. Features and development of Coot.
739   *Acta Crystallogr. D Biol. Crystallogr.* **66**, 486–501 (2010).

740 76. Long, F. *et al.* AceDRG: a stereochemical description generator for ligands. *Acta*
741   *Crystallogr D Struct Biol* **73**, 112–122 (2017).

742 77. Bricogne, G. *et al.* BUSTER version 2.10. 0. *Cambridge, United Kingdom: Global Phasing*
743   *Ltd* (2011).

744

Acknowledgments